IEEE Access
Multidisciplinary | Rapid Review | Open Access Journal

Received 23 January 2024, accepted 17 February 2024, date of publication 22 February 2024, date of current version 29 February 2024.

Digital Object Identifier 10.1109/ACCESS.2024.3368885

RESEARCH ARTICLE

Flexible Photonic Sensors: Investigation of an Approach Based on Ratiometric Power in Few-Mode Waveguides for Bending Measurement

ANDREA ANNUNZIATO[1], MIKE GODFREY[2], FRANCESCO ANELLI[1], (Student Member, IEEE), JANICE DULIEU-BARTON[3], CHRISTOPHER HOLMES[4], AND FRANCESCO PRUDENZANO[1], (Member, IEEE)

[1]Department of Electrical and Information Engineering, Politecnico di Bari, 70125 Bari, Italy
[2]School of Engineering, University of Southampton, SO17 1BJ Southampton, U.K.
[3]School of Civil Aerospace and Mechanical Engineering, University of Bristol, BS8 1UG Bristol, U.K.
[4]Optoelectronics Research Centre, University of Southampton, SO17 1BJ Southampton, U.K.

Corresponding author: Francesco Prudenzano (francesco.prudenzano@poliba.it)

This work was supported in part by the European Union under the Italian National Recovery and Resilience Plan (NRRP) of NextGenerationEU, "Telecommunications of the Future" (PE00000001—Program "RESTART," CUP: D93C22000910001) through Antennas and Devices foR mixing, dEtection And Manipulation of mmWaves (DREAMS); in part by Ministero dell'Istruzione e del Merito (MIUR) "Agriculture Green and Digital—AGREED," PNR 2015/2020, under Grant ARS01_00254; in part by the H2020-ICT-37-2020 "Photonic Accurate and Portable Sensor Systems Exploiting Photo-Acoustic and Photo-Thermal Based Spectroscopy for Real-Time Outdoor Air Pollution Monitoring—PASSEPARTOUT" under Grant 101016956; in part by MIUR PRIN 2022, NRPP—DD [27-07-2023—InnoVative tEchnoloGies for non-invasivE assessmenT of plAnt healTh conditIon to support precisiOn farmiNg (VEGETATION)] under Grant 1181; in part by the Engineering and Physical Sciences Research Council (EPSRC) "Roll-2-Roll (R2R) Manufacture of Multilayer Planar Optics," under Grant EP/V053213/1; and in part by the EPSRC "Future Composites and Manufacturing Hub," under Grant EP/P006701/1.

ABSTRACT A novel approach to monitor the degree of bending via flexible photonics devices, using ratiometric power variation in a few-mode optical waveguide, is proposed. To demonstrate its feasibility, a sensor exploiting a Bragg grating, approximately aligned to the neutral axis, is designed, fabricated and characterized. The reduced thickness of the proposed planar photonic sensor is uniquely limited by optical confinement requirements, enabling for an ultra-thin and highly flexible planar device, based on all-glass platform. Finite Element Method, Beam Propagation Method and Coupled Mode Theory are employed in the design to model the electromagnetic and mechanical phenomena occurring during the three-point bending test. The experiment demonstrates that the planar device withstands tight curvature without mechanical failure. The device shows that by increasing the bending the reflected power from the fundamental mode decreases and the reflected power from the higher order mode increases. The measured ratiometric power sensitivity versus displacement is $K_{P_R} = -0.78$ dB/mm with negligible variation over a 40°C thermal range. Therefore, exploiting both the Bragg wavelength shift and the mode optical power change, the proposed sensor can be employed for multiparameter sensing purposes, e.g. simultaneous temperature and curvature monitoring.

INDEX TERMS Coupled mode theory, flexible photonics, bending, optical fiber sensor, Bragg grating.

I. INTRODUCTION

Flexible photonics is a rapidly advancing research field. Traditional rigid devices in planar optics can be refined through controlled thinning, adding the ability to flex while preserving their essential functionality. This innovative class of photonic devices has been successfully fabricated on a number of substrates, as extensively documented in various recent articles [1], [2], [3], [4], [5], [6], [7]. Specifically, polymer waveguides demonstrate remarkable flexibility,

The associate editor coordinating the review of this manuscript and approving it for publication was S. M. Abdur Razzak.

enabling significant levels of curvature, twisting, and stretching [6], [8]. However, it is worth noting that the refractive index contrast may not consistently meet the demands for robust optical field confinement and that polymers can exhibit poor performance when subjected to harsh environments such as elevated temperatures or exposure to solvents [6].

Recent studies have also explored the integration of glass onto polymer structures [9], [10], aligning with the growing focus on flexible photonics based on all-glass substrates and components [11], [12], [13]. Glass substrates excel for their optical performance, exceptional chemical properties, thermal resilience, and superior refractive index contrast compared to polymer waveguides [12], [13]. The higher elastic moduli exhibited by glass materials, as opposed to plastics and polymers, contribute to their inherent rigidity in a solid state. The bendability of all glass photonic devices significantly depends on the thickness of the material. This is the main factor affecting the ability of glass to adapt to a range of curvature configurations. Indeed, for materials that have a low tensile strength, such as doped silica, reducing thickness can also increase the total degree of flexure prior to failure.

For optical-based bend sensors, the overall thickness of the device typically arises from the established practice, wherein the waveguide is traditionally situated apart from the neutral axis. Here, a minimum thickness becomes necessary to establish the offset from the neutral axis and ensure optical modes confinement. If the neutral axis is aligned or closely aligned with the core, the sensor tends to exhibit minimal or no detectable response.

In this paper, a novel approach for curvature monitoring via all-glass flexible sensors, using ratiometric power variation between the fundamental and higher order mode in a bimodal optical waveguide, is proposed. As proof of concept, a flexible photonic bend sensor (see Fig. 1), is designed, fabricated through Flame Hydrolysis Deposition (FHD) and characterized via three-point bending test [18]. Notably, the channel waveguide is deliberately aligned slightly off-axis, a departure from the conventional approach for bend sensors. The optical characteristic of the Bragg grating is comprehensively examined both theoretically and experimentally, including analyses of Bragg wavelength shifts and alterations in optical mode power, particularly under the influence of pure bending. The designed sensor has a reduced thickness that minimizes the internal strain values, allowing a strong extension of the typical sensing range of cylindrical optical fiber, up to 110 m^{-1} without the use of low stiffness materials [19], [20]. The obtained results show that this novel approach could be exploited for the development of innovative optical sensors, allowing the simultaneous temperature and curvature monitoring, or, more in general, multiparameter monitoring. Progress in this domain is expected to influence fields including soft robotics, medicine, and the monitoring of engineered structures [4], [15], [16], [17], [21], [22].

After the Section I, the paper is organized as follows: Section II illustrates the electromagnetic design and mechanical performance investigation of the sensor; Section III describes the sensor fabrication and the comparison between numerical and experimental results; Section IV provides the conclusions and the discussion on the future prospects.

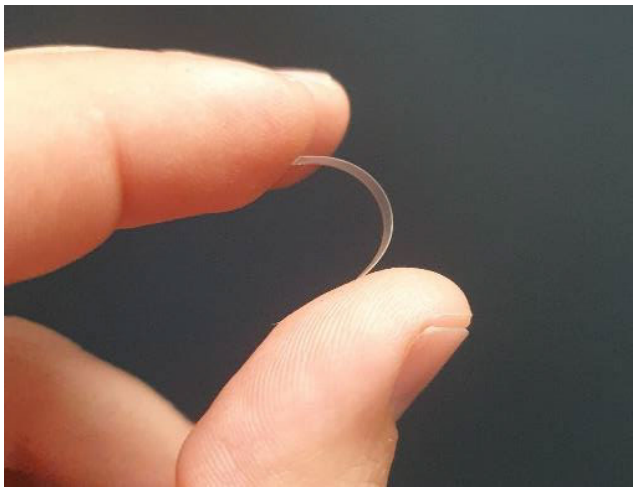

FIGURE 1. Flexible planar photonic chip in doped silica fabricated through flame hydrolysis deposition.

II. ELECTROMAGNETIC AND MECHANICAL MODELING

A. DESIGN APPROACH

The design of the flexible photonic sensor is developed via 2D-Finite Element Method (FEM) electromagnetic modal analysis, using the COMSOL Multiphysics® Wave Optics module. Then, the flexible photonic sensor is modeled via 3D-FEM, using the COMSOL Multiphysics® Structural Mechanics module, to simulate the three-point bending test. The optical response of the Bragg grating, under three-point bending, is investigated through electromagnetic and mechanical analyses. The mechanical analysis allows to determine the maximum displacement, the curvature profile, and the strain distribution. The calculated curvature profile is used in the 3D-BPM modeling (Beam Propagation Method, BeamProp®-RSOFT Design®) to assess power mode mixing in addition to the Coupled Mode Theory (CMT). It is well known that in multimode waveguides, bending induces mode coupling and optical power exchange amongst other phenomena. The strain distribution, the electromagnetic field profile, and the powers of the propagating modes are employed as inputs to an in-house MATLAB® code based on CMT [23]. This combines the influence of the bending on refractive index distribution, grating period, and coupling coefficients. CMT is exploited to compute the reflection spectra and the Bragg wavelength shift of the gratings [14].

Three Bragg gratings, namely #G1, #G2, and #G3, are designed following the aforesaid approach. An exhaustive electromagnetic investigation is focused on the Bragg grating #G2, constituting the flexible sensor, which is subjected to an almost constant curvature along the entire grating length. The numerical results agree with the experiment and explain

the optical response of both #G2 and the other two Bragg gratings #G1 and #G3 designed and fabricated only to better explain the sensor behavior.

B. ELECTROMAGNETIC DESIGN AND MODAL INVESTIGATION

Generally, fiber Bragg gratings can be adopted to infer the level of bending by exploiting an off-axis core and observing the Bragg wavelength shift. To investigate the feasibility of the sensor for the monitoring of two parameters, e.g. the curvature and the temperature, a channel waveguide with two propagating modes is designed. The electromagnetic design of the flexible photonic sensor with a slight off-axis core is carried out. Figure 2 shows a not-to-scale sketch of the flexible sensor cross-section. The total thickness is $t_{fp} = 60\ \mu$m and the total width is $w_{fp} = 1$ mm. The thickness t_{fp} is chosen as a trade-off, to provide both a low level of surface stress and a suitable electromagnetic field confinement when the sensor is bent. The sensor is multi-layered, comprising overclad, core, and underclad. The underclad thickness is slightly larger than the overclad so that the core layer is 1.5 μm offset from the central neutral axis of the sensor.

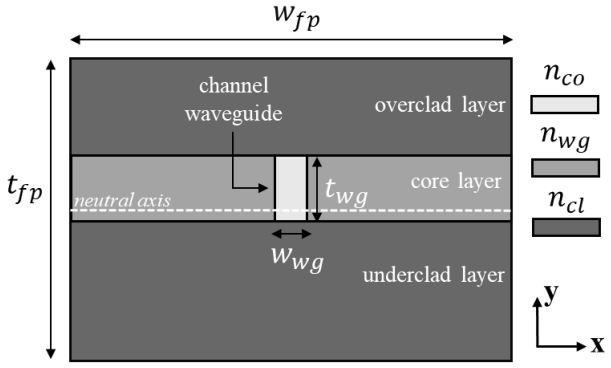

FIGURE 2. Sketch of the flexible sensor. The channel waveguide (light gray colored), in which the gratings are inscribed, is written in the central core layer and it is slightly off-axis with respect to the neutral axis.

The channel waveguide is rectangular, and it is written within the core layer. Its width is $w_{wg} = 7\ \mu$m and its thickness is identical to the one of the core layer, $t_{co} = t_{wg} = 9\ \mu$m. The underclad and overclad layers are made of identical silica glass composition and uniform refractive index distribution $n_{cl} = 1.4452$ at the wavelength $\lambda = 1553$ nm. The core layer refractive index is $n_{co} = 1.4645$ at the wavelength $\lambda = 1553$ nm. At the same wavelength, the channel waveguide refractive index is $n_{wg} = 1.4695$, obtainable by adopting direct UV Writing (DUW) manufacturing technique. Both the core layer and the channel waveguide have a step-index profile distribution. The refractive index wavelength dispersion is modeled via a suitable Sellmeier equation [24]. The norm of the electric field E of the fundamental and high (second) order mode, i.e. the spatial modes E_{11}, E_{21}, is reported in Fig. 3.

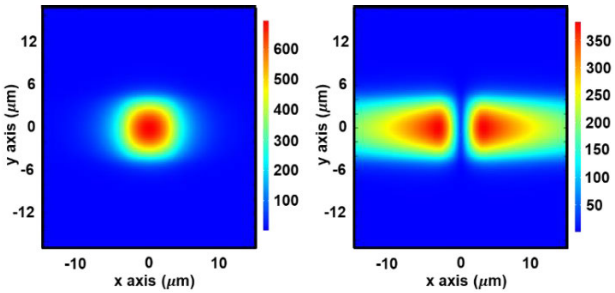

FIGURE 3. Norm of the electric field E of the fundamental E_{11} and high order mode E_{21}. The coordinates (0; 0) refer to the center of the waveguide.

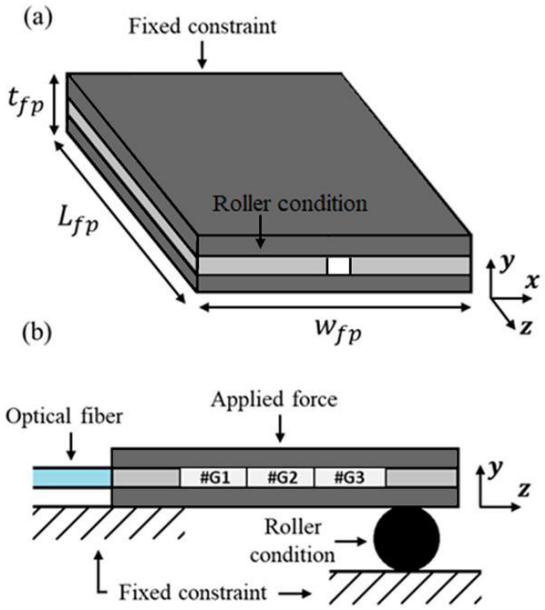

FIGURE 4. (a) Sketch of the boundary conditions and applied forces to the 3D-FEM modeled flexible photonic sensor for three-point bending test simulation; (b) schematic representation of the set-up and Bragg gratings locations.

C. MECHANICAL INVESTIGATION: THREE-POINT BENDING TEST

To numerically investigate the sensor response to the three-point bending test, the multi-layered glass platform described in Section II-B and having a length $L_{fp} = 60$ mm, see Fig. 4 (a), is 3D-modeled. The employed mechanical parameters, such as Poisson's ratio $\nu = 0.17$ and Young's modulus E_{cl}, have been measured through nano-indentation tests [21]. The underclad and overclad compositions are identical, with Young's modulus $E_{cl} = 40$ GPa. The core layer is stiffer than the cladding layers and its Young's modulus is $E_{co} = 62$ GPa. The boundary conditions and the applied forces are set in the 3D-FEM model as reported in the sketch of Fig. 4 (a), (b). Moreover, Fig. 4 (b) is a schematic of the set-up, highlighting the position of the three Bragg gratings, namely #G1, #G2, #G3, and the position where the force F is applied. A fixed constraint condition is applied on the left

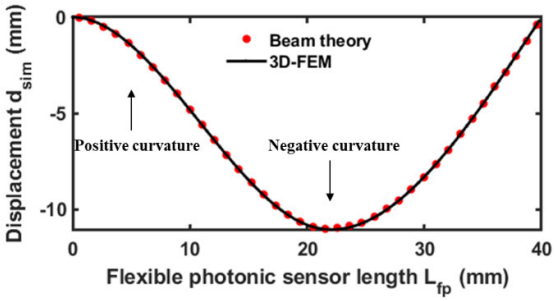

FIGURE 5. Displacement profile as a function of the flexible photonic sensor length L_{fp} considering the applied force F_5.

boundary of the flexible photonic sensor, while, on the right, a simply supported boundary condition is imposed.

The force F acts perpendicularly to the longitudinal axis (z-axis), at the centre of the Bragg grating #G2. A free tetrahedral mesh is employed, consisting of $M_{3D-FEM} = 168442$ domain elements. Three-point bending test is simulated by considering the force values $F_i = [0\text{ mN}, 3.3\text{ mN}, 6.6\text{ mN}, 9.8\text{ mN}, 12\text{ mN}]$ with $i = 1 \rightarrow 5$.

The simulated maxima displacements d_{sim}, for each force value F_i, are respectively $d_{sim} = [0\text{ mm}, 3\text{ mm}, 6\text{ mm}, 9\text{ mm}, 11\text{ mm}]$. Figure 5 plots the simulated displacement of the flexible photonic sensor versus its length L_{fp} due to the force F_5, i.e. the maximum applied force value; the convention used to define the curvature sign is indicated in Figure 5. The displacement d_{sim} obtained from the 3D-FEM model (black solid curve) perfectly agrees with that obtained by classical beam theory (red dotted markers) [25]. The 3D-FEM approach allows a multiphysics investigation including the internal strain calculation. Figure 6 illustrates the curvature radius C_R as a function of the cumulative arc length S, for the case of maximum displacement $d_{sim} = 11$ mm. The curvature radius is evaluated by considering the curvature equation $C_R = |\left(1+\dot{y}^2\right)^{\frac{3}{2}}/\ddot{y}|$ where $\dot{y}$ and $\ddot{y}$ are the first and second order derivative of the displacement profile function. The values of the curvature radius C_R, are then used for 3D-BPM modeling.

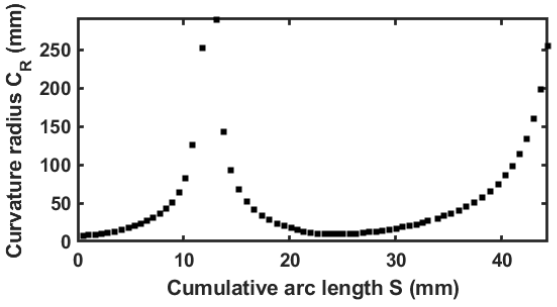

FIGURE 6. Curvature radius C_R vs cumulative arch length S considering the applied force F_5.

D. POWER MODE MIXING

The mode optical power exchange between the propagating modes in a bent optical fiber/waveguide is analysed via 3D-BPM, which exploits the conformal mapping method [26]. The conformal mapping is used to map the cross-sectional refractive index n_c of a curved optical waveguide, into a straight one. If the size of the flexible photonic sensor is very small compared to the applied curvature radius C_R, a straight equivalent waveguide, with a novel cross-sectional refractive index $n_m = n_c\left(1 + x_p/C_R\right)$, can be modeled [26], [27]. The distance from the optical waveguide centre is indicated with x_p, while n_c is the cross-sectional refractive index when the sensor is unperturbed, i.e. not bent. 3D-BPM approach does not consider the effect caused by the strain field on the refractive index n_c. This further effect is taken into account in Section II-E for the evaluation of the Bragg grating spectra, using stress-optic relations [28]. For each value of d_{sim}, the curvature radius C_R versus the cumulative arc length S is exploited by 3D-BPM to calculate the cross-sectional refractive index n_m and to assess the power mode mixing. To simulate the butt coupling with a single mode optical fiber, a Gaussian beam profile is considered as an input optical field.

The grid resolution of the simulation is $M_{BPM,t} = 0.1\ \mu$m and $M_{BPM,l} = 0.25\ \mu$m respectively for transverse (x-y axis) and longitudinal direction (z axis). By considering the maximum displacement $d_{sim} = 11$ mm, the power mode mixing investigation for the grating #G2 demonstrates (as it will be shown in Section II-E) that the simulated peak power $P_{s,hom}$ of the high order mode increases of $\Delta P_{s,hom} = 3.4$ dBm at the expense of the peak power $P_{s,fun}$ of the fundamental mode.

E. BRAGG GRATING SPECTRUM EVALUATION

The 2D-FEM modal analysis is carried out by using the stress-optic relations and the strain distribution within the flexible photonic sensor, derived from the 3D-FEM mechanical investigation. To solve CMT, the transversal coupling coefficients $K^t(z)$ are calculated considering the effective refractive indices n_{eff} and the electromagnetic field profiles E of the two modes propagating along the z axis (along both positive and negative directions) [23]:

$$K^t_{\pm}(z) = \frac{w_f}{4}\iint_{core} \Delta\epsilon\,(x,y,z)\,E^t_{+}(x,y,z)\,\bar{E^t_{-}}(x,y,z)dxdy \tag{1}$$

where w_f is the angular frequency, $E^t(x,y,z)$ is the transversal electromagnetic field profile, $\Delta\epsilon\,(x,y,z)$ is the dielectric perturbation which relies on refractive index modulation. The 3D-BPM is employed to calculate the input power of the two guided modes in CMT model [23]. To compute the reflection spectrum of grating #G2, the approach is executed for each displacement d_{sim}; the wavelength range is from $\lambda = 1514$ nm to $\lambda = 1520$ nm with a wavelength step $\Delta\lambda_{step} = 5$pm. The effective refractive index of the fundamental mode is $n_{eff,fun} = 1.46618$ and that of the second order mode is $n_{eff,hom} = 1.46291$ at the wavelength $\lambda = 1553$ nm. The designed uniform Bragg grating has a sinusoidal modulation with an amplitude $\Delta n_{BG} = 2\times10^{-4}$ and a length

$L = 12$ mm. The nominal grating period of #G2, when the planar sensor is not subjected to curvature, is $\Lambda_{\#G2} = 0.51774\ \mu$m.

This value is selected to obtain the mode matching between the forward and backward fundamental mode around the wavelength $\lambda = 1519$ nm. For completeness, the grating period of Bragg grating #G1, and #G3 were selected to obtain the resonant wavelengths of the fundamental mode at $\lambda_{\#G1} = 1528$ nm and $\lambda_{\#G3} = 1588$ nm.

Figure 7 reports the simulated reflection spectrum when grating #G2 is unperturbed and when a displacement $d_{sim} = 11$ mm is applied, respectively. The propagating modes interact with the Bragg grating #G2 producing two resonant wavelengths. Moreover, Fig. 7 shows that the applied bending produces i) a power exchange between the two modes and ii) a blue shift of the resonant wavelengths. The results demonstrate a variation of the Bragg wavelength for both the fundamental and high order mode, reaching the maximum Bragg wavelength shift $\Delta\lambda_{s,fun} = -250$ pm and $\Delta\lambda_{s,hom} = -240$ pm, respectively.

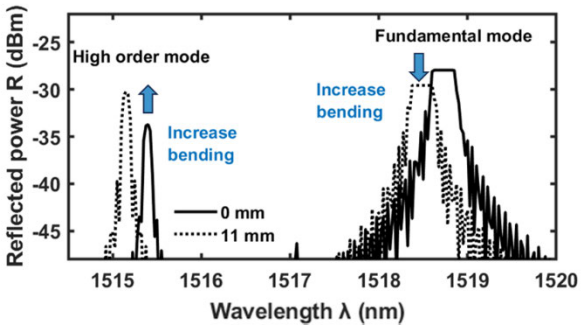

FIGURE 7. Simulated reflection spectrum of the Bragg grating #G2, unperturbed (solid curve) and with displacement d_{sim}=11*mm* (dotted curve); length of the Bragg grating L= 12*mm*, refractive index modulation of the Bragg grating $\Delta n_{BG} = 2\times10^{-4}$.

III. FABRICATION AND CHARACTERIZATION

A. FLEXIBLE PHOTONIC SENSOR FABRICATION

The flexible glass substrate is fabricated using FHD. This process involves the sequential deposition of three doped silica layers (overclad, core and underclad), onto a rigid sacrificial silicon wafer (diameter $d_{sw} = 152$ mm, thickness $t_{sw} = 1$ mm, p-doped [100]). The silicon had a thermally grown wet oxide layer, of thickness $t_{wo} = 6\ \mu$m, used to avoid chemical reaction between the deposited doped silica layers and the silicon substrate. The use of equal compositions for the underclad and overclad, balances the stress differentials on both the sides of the flexible substrate and reduces intrinsic bend when released from the sacrificial substrate. The underclad and overclad layers are processed with flow rates of $SiCl_4$ at 137 sccm, BCl_3 at 70 sccm and PCl_3 at 31 sccm through a hydrogen-oxygen flame with flow rate 6.5 L/min and 1.5 L/min, respectively. The fabrication of the core layer is made with flow rates of $SiCl_4$ at 123 sccm, $GeCl_4$ at 130 sccm, BCl_3 at 16 sccm through a hydrogen-oxygen flame with flow rate 5.4 L/min and 2.7 L/min. After each FHD layer, the deposited soot requires high temperature consolidation. This was achieved within a furnace, flowing O_2 at rates of 1.9 L/min and consolidating at temperatures $T_{co} = 1360$°C and $T_{cl} = 1250$°C, for the core layer and cladding layers respectively. The final processing step, to create the flexible photonic platform, is obtained by removing the rigid silicon substrate through a physical machining process [18].

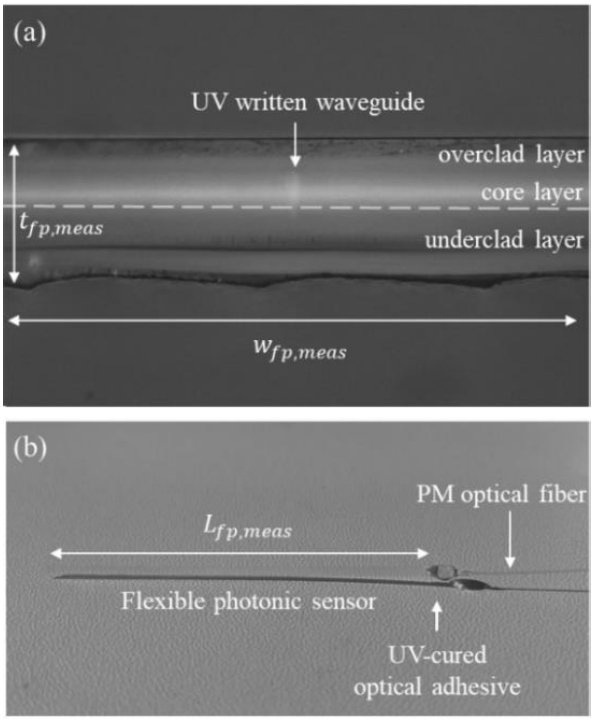

FIGURE 8. (a) Cross-section of the flexible photonic sensor captured via microscope camera; (b) flexible photonic sensor coupled to a polarization maintaining optical fiber via UV-cured optical adhesive.

Figure 8 (a) shows the cross-section of the fabricated device, captured via microscope camera. The flexible photonic sensor has a measured width of $w_{fp,meas} \sim 1$ mm, thickness $t_{fp,meas} \sim 58\ \mu$m and length $L_{fp,meas} \sim 60$ mm. The thickness of the underclad is greater than that of the overclad. A key feature of the design is that the core layer is not centred on the neutral axis, but it is offset.

The measured core layer thickness $t_{co,meas}$ differs slightly with respect to the desired t_{co}, due to dopant diffusion induced by the high temperature process involved. Figure 8 (b) shows the flexible photonic sensor coupled via UV-cured optical adhesive with a single mode polarization maintaining (PM) optical fiber. The refractive indices are measured, through a prism coupler, at the wavelength $\lambda = 1553$ nm. The underclad and overclad layers have a measured refractive index $n_{cl} = 1.445$, while the core layer has a measured refractive index $n_{co} = 1.469$.

B. BRAGG GRATINGS INSCRIPTION

The DUW technique is able to simultaneously inscribe the channel waveguide and the three Bragg gratings within the UV photosensitive core layer [29]. The Bragg gratings are

written at different positions, along the length of the device, as shown in Fig. 4 (b). They have a length $L = 12\ mm$ and a uniform apodization profile, refractive index modulation of the Bragg grating $\Delta n_{BG} = 2 \times 10^{-4}$. Moreover, they are pseudo-randomly ordered, such that the spectral sequence does not correlate with spatial sequence. The measured resonant wavelengths of the fundamental mode are $\lambda_{\#G1} = 1528\ nm$, $\lambda_{\#G2} = 1519\ nm$ and $\lambda_{\#G3} = 1588\ nm$. The reflected power versus the wavelength for the three unperturbed Bragg gratings is shown in Fig. 9. According to the electromagnetic design, the waveguide supports two modes of propagation, since two resonant peaks for each grating are evident.

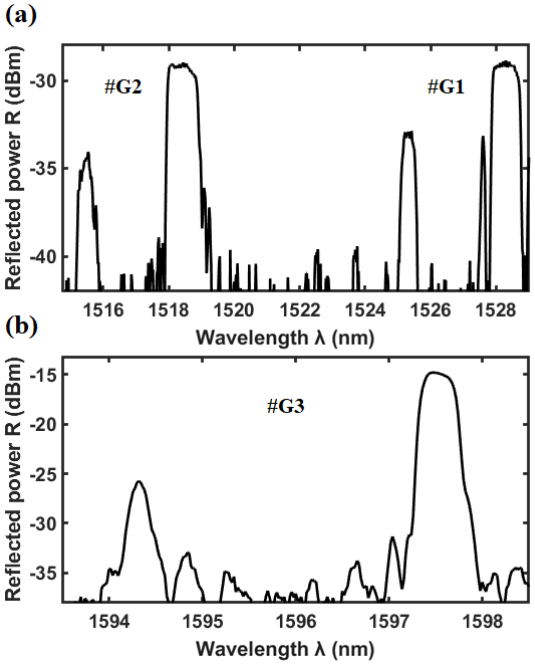

FIGURE 9. Measured reflection spectra of the unperturbed Bragg gratings (a) #G1, #G2 and (b) #G3; length of the Bragg grating $L = 12mm$, refractive index modulation of the Bragg grating $\Delta n_{BG} = 2 \times 10^{-4}$.

C. THREE-POINT BENDING TEST AND OPTICAL MEASUREMENT

The flexible photonic sensor was loaded in a mechanical test rig to observe the optical response when subjected to large deflections. An Instron E1000 electromechanical test machine is used to apply three-point bending. The fixture comprises three steel rollers having a diameter $d_{roll} = 6$ mm, each separated by a distance $s = 20$ mm. The upper roller is used to apply the displacement and was attached to the actuator as shown in Fig. 10. The side which is optically coupled to the fiber (left-hand side in Fig. 10) was secured using a tape to limit influence from optical fiber movement.

The flexible photonic sensor was subjected to an incremental displacement d, from $d = 0$ mm (i.e. unperturbed) to $d = 11$ mm. The optical measurements were carried out during the three-point bending test, using the set-up shown in Fig. 11. A negative Bragg wavelength shift in the pm range was

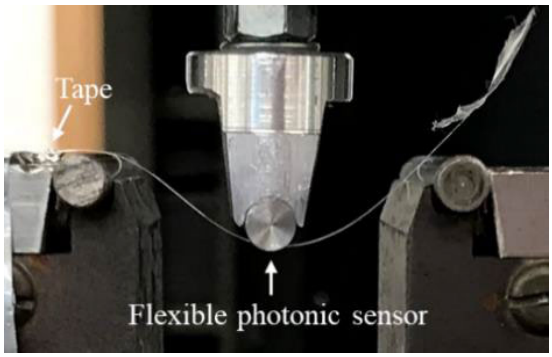

FIGURE 10. Photograph of the experimental set-up. Centre-to-centre separation of rollers $s = 20mm$, diameter of rollers $d_{roll} = 6mm$.

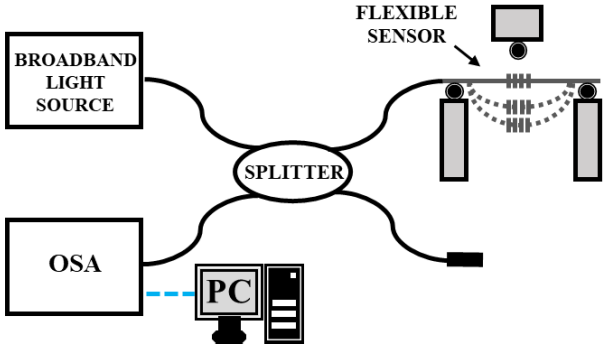

FIGURE 11. Experimental set-up employed for spectra measurements.

obtained [14]. Grating #G2 is positioned at the loading point where the displacement and the strains are the largest and it is subjected to a curvature with negative concavity (see Fig. 5). Therefore, compared with the other gratings, it produces the greatest wavelength shifts. The maximum measured Bragg wavelength shift $\Delta\lambda_m$, for the fundamental and high order mode, are $\Delta\lambda_{m,fun} = -264$ pm and $\Delta\lambda_{m,hom} = -223.5$ pm, respectively. There is an increase of the measured peak power $\Delta P_{m,hom} = +4$ dBm for the high order mode, for a displacement $d = 11$ mm. The optical measurements of all the gratings optical responses, for increasing displacement $d = [0 - 11]$ mm of the central roller, are reported in Fig. 12 and Fig. 13.

Figures 12 (a) and (b) illustrate the measured Bragg wavelength shifts $\Delta\lambda_m$, of the fundamental mode (triangle markers) and high order mode (cross markers) for the gratings #G1 and #G3. Figures 12 (c) and (d) report the comparison between the simulated (dotted line) and measured Bragg wavelength shifts $\Delta\lambda$, of the fundamental mode (triangle markers) and high order mode (cross markers), of the grating #G2. As previously underlined, the grating #G2 constitutes the sensor, the gratings #G1 and #G3 are considered for a critical discussion of the obtained results. It is evident that the numerical results perfectly agree with the experimental measurements. By analysing the wavelength shifts reported in Fig. 12, all the gratings and both the propagating modes, show a shift of the resonant peaks towards smaller wavelengths. Since grating #G2 lies along

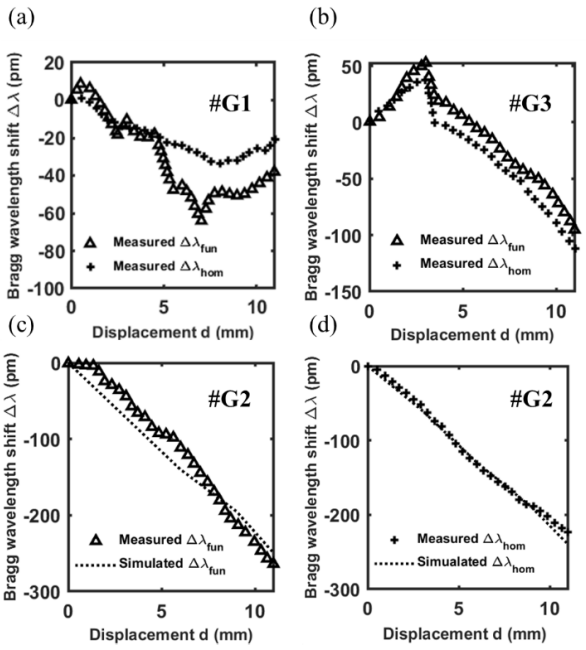

FIGURE 12. Measured Bragg wavelength shifts $\Delta\lambda_m$, of the fundamental mode (triangle markers), high order mode (cross markers) for (a) the gratings #G1 and (b) #G3. (c) Comparison between the simulated (dotted curve) and measured (triangle markers) Bragg wavelength shift $\Delta\lambda_{fun}$ of the fundamental mode, (d) comparison between the simulated (dotted curve) and measured (cross markers) Bragg wavelength shift $\Delta\lambda_{hom}$ of the high order mode, for the grating #G2.

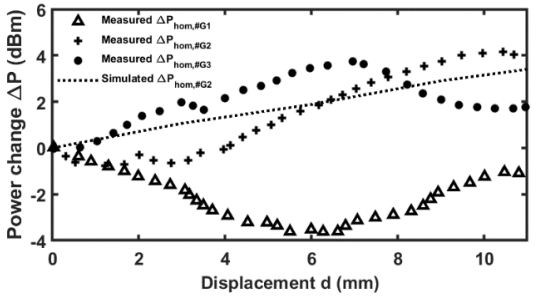

FIGURE 13. Measured peak power change $\Delta P_{m,hom}$ versus the displacement d for the high order mode of the grating #G1 (triangle markers), #G2 (cross markers), #G3 (circle markers) and simulated peak power change $\Delta P_{s,hom}$ for the grating #G2 (dotted curve).

the region of maximum and constant negative curvature, the Bragg wavelength shift $\Delta\lambda_m$ is negative with a linear trend that is larger than that of the gratings #G1 and #G3. Regarding the grating #G1, it is positioned in a region where two curvatures with opposite signs are present. This provides an explanation for the wavelength shift reaching $\Delta\lambda_{m,fun} = -38$ pm, $\Delta\lambda_{m,hom} = -20.6$ pm at the maximum central displacement $d = 11$ mm. The right end of the flexible photonic sensor is unbonded, thus also the grating #G3 is subjected to a negative curvature. In this case, the displacement and the strains are lower than that occurring at the loading point, where the grating #G2 is located. The maximum measured Bragg wavelength shift for the grating #G3 is $\Delta\lambda_{m,fun} = -95.2$ pm, $\Delta\lambda_{m,hom} = -112$ pm. Ultimately, the grating #G2, subjected to curvature, provides Bragg wavelength shift sensitivities $K_{\lambda,fun} = -2.4$ pm/m^{-1}, $K_{\lambda,hom} = -2.1$ pm/m^{-1}.

Figure 13 illustrates the measured peak power change $\Delta P_{m,hom}$ for the high order mode of the grating #G1 (triangle markers), #G2 (cross markers) and #G3 (circle markers) as a function of the displacement d. The simulated peak power change $\Delta P_{s,hom}$ of the high order mode of the grating #G2 (dotted line) is in good agreement with the measured value. The power trend of the high order mode of gratings #G1 and #G3 (symmetric about the loading point) is comparable but with opposite changes in power. Both the gratings reach the maximum peak power change $\Delta P_{m,hom}$ at a displacement of $d = 6$ mm.

The power exchange between the two propagating modes can be exploited to infer the level of bending of the grating #G2, by using the ratiometric power P_R. Where P_R is defined as the ratio between the peak power reflected by the fundamental mode $P_{m,fun}$ and the high order mode $P_{m,hom}$. In Fig. 14 the measured ratiometric power P_R of the grating #G2 versus the displacement d (cross markers) is reported. The red dashed line is the linear fit of the experimental curve. The sensor exhibits a linear response between $d = 2$ mm and $d = 10$ mm with a ratiometric power sensitivity being $K_{P_R} = -0.78$ dB/mm. The almost flat response between $d = 0$ mm and $d = 2$ mm, can be addressed to an unwanted initial deflection of the sensor. It is worth noting that, over a 40°C thermal range, power change shows negligible variation, thus it is not affected by environment temperature. The measured thermo-optic Bragg shift sensitivity is approximately $K_T = 11.5$ pm/K.

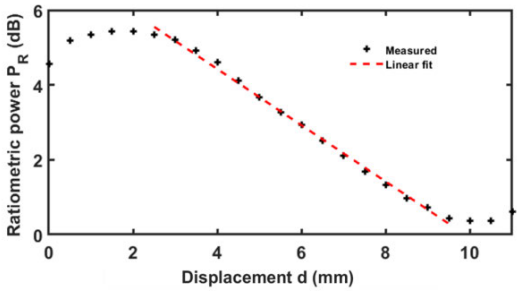

FIGURE 14. Ratiometric power P_R versus the displacement d for the grating #G2 (cross markers). The red dashed line is the linear fit of the curve.

D. DISCUSSION OF RESULTS

The focus of this paper is the demonstration of a novel approach to infer level of bending, based on ratiometric power change, between the peak power reflected by fundamental and high order mode. Table 1 reports a comparison with other Bragg curvature sensors which exhibit very high performances and include different approaches: multimode interference [30], embedding in silicone substrate [31], polymeric optical fibers with eccentric core [32], multicore optical fibers [33], or tilted FBGs [34]. In particular, multimode interference [30] requires a more sophisticated measurement approach, with excitation of a number of modes; embedded in

TABLE 1. State-of-art comparison between flexible sensors.

Reference	Thickness	Maximum curvature	K_λ	K_{P_R}	K_T	T compensation
[30]	125 µm	–	–	2.1 dB/mm	–	no
[31]	5 mm	80 m^{-1}	1.64 pm/m^{-1}	–	–	no
[32]	230 µm	22.7 m^{-1}	63 pm/m^{-1}	–	–	no
[33]	150 µm	11 m^{-1}	59.47 pm/m^{-1}	–	–	yes
[34]	–	15.5 m^{-1}	–	0.74 dB/m^{-1}	–	yes
This work	58 µm	110 m^{-1}	2.4 pm/m^{-1}	0.78 dm/mm	11.5 pm/K	yes

silicone sensor [31] exhibits higher thickness; polymeric optical fibers [32] show higher confinement losses due to lower refractive index changes; [33], [34] show high sensitivities but smaller measurement range. The proposed proof of concept shows the following strength points: i) the minimum thickness, ii) the maximum curvature, iii) exploitation of the ratiometric power, which is immune to temperature variation, iv) immunity to power fluctuation of light source, due to the intrinsic compensation of the measurement technique, v) simultaneous measurement of bending and temperature. These results encourage further work towards the refinement in design/fabrication of other devices based on the same techniques.

IV. CONCLUSION

A new approach for bending monitoring via flexible photonics is proposed by considering both the ratiometric power between the peak power reflected by fundamental and higher order mode and Bragg wavelength shift. A sensor is fabricated to validate the approach. In particular, a comprehensive optomechanical design and characterization of the flexible photonic sensor is reported. Compared to other fiber optic curvature sensors, the proposed solution minimizes the total thickness of the substrate, enabling the achievement of higher degree of bending. The results indicate that the wavelength shift depends on the sign of applied curvature. The experiments agree with simulations and show that the proposed flexible sensor can withstand very high curvatures up to 110m^{-1}. The grating #G2 provides Bragg wavelength shift sensitivities $K_{\lambda,fun} = -2.4$ pm/m^{-1}, $K_{\lambda,hom} = -2.1$ pm/m^{-1} and ratiometric power sensitivity $K_{P_R} = -0.78$ dB/mm. Regarding thermal characterization of the sensor, negligible variation over a 40°C range has been observed in terms of power change. The thermo-optic sensitivity is approximately $K_T = 11.5$ pm/K. The values of Bragg wavelength shift, and temperature-independent ratiometric optical power change can be exploited for simultaneous temperature and curvature sensing, paving the way for the construction of a new class of multiparameter sensors.

REFERENCES

[1] M. De Carlo, F. De Leonardis, R. A. Soref, and V. M. N. Passaro, "Design of an exceptional-surface-enhanced silicon-on-insulator optical accelerometer," *J. Lightw. Technol.*, vol. 39, no. 18, pp. 5954–5961, Sep. 2021.

[2] J. Missinne, S. Kalathimekkad, B. Van Hoe, E. Bosman, J. Vanfleteren, and G. Van Steenberge, "Stretchable optical waveguides," *Opt. Exp.*, vol. 22, no. 4, pp. 4168–4179, 2014.

[3] S. Geiger, J. Michon, S. Liu, J. Qin, J. Ni, J. Hu, T. Gu, and N. Lu, "Flexible and stretchable photonics: The next stretch of opportunities," *ACS Photon.*, vol. 7, no. 10, pp. 2618–2635, Oct. 2020.

[4] W. Peng and H. Wu, "Flexible and stretchable photonic sensors based on modulation of light transmission," *Adv. Opt. Mater.*, vol. 7, no. 12, pp. 1–27, Jun. 2019.

[5] L. Li, H. Lin, J. Michon, Y. Huang, J. Li, Q. Du, A. Yadav, K. Richardson, T. Gu, and J. Hu, "A new twist on glass: A brittle material enabling flexible integrated photonics," *Int. J. Appl. Glass Sci.*, vol. 8, no. 1, pp. 61–68, Mar. 2017.

[6] J. Hu, L. Li, H. Lin, P. Zhang, W. Zhou, and Z. Ma, "Flexible integrated photonics: Where materials, mechanics and optics meet [invited]," *Opt. Mater. Exp.*, vol. 3, no. 9, pp. 1313–1331, 2013.

[7] G. C. Righini, J. Krzak, A. Lukowiak, G. Macrelli, S. Varas, and M. Ferrari, "From flexible electronics to flexible photonics: A brief overview," *Opt. Mater.*, vol. 115, May 2021, Art. no. 111011.

[8] H. Zuo, S. Yu, T. Gu, and J. Hu, "Low loss, flexible single-mode polymer photonics," *Opt. Exp.*, vol. 27, no. 8, pp. 11152–11159, 2019.

[9] L. Li, H. Lin, S. Qiao, Y. Zou, S. Danto, K. Richardson, J. D. Musgraves, N. Lu, and J. Hu, "Integrated flexible chalcogenide glass photonic devices," *Nature Photon.*, vol. 8, no. 8, pp. 643–649, Aug. 2014.

[10] L. Li, H. Lin, Y. Huang, R.-J. Shiue, A. Yadav, J. Li, J. Michon, D. Englund, K. Richardson, T. Gu, and J. Hu, "High-performance flexible waveguide-integrated photodetectors," *Optica*, vol. 5, no. 1, pp. 44–51, 2018.

[11] S. Huang, M. Li, S. M. Garner, M.-J. Li, and K. P. Chen, "Flexible photonic components in glass substrates," *Opt. Exp.*, vol. 23, no. 17, pp. 22532–22543, 2015.

[12] O. Sayginer, E. Iacob, S. Varas, A. Szczurek, M. Ferrari, A. Lukowiak, G. C. Righini, O. S. Bursi, and A. Chiasera, "Design, fabrication and assessment of an optomechanical sensor for pressure and vibration detection using flexible glass multilayers," *Opt. Mater.*, vol. 115, May 2021, Art. no. 111023.

[13] G. Macrelli, A. K. Varshneya, and J. C. Mauro, "Ultra-thin glass as a substrate for flexible photonics," *Opt. Mater.*, vol. 106, Aug. 2020, Art. no. 109994.

[14] F. Anelli, A. Annunziato, M. Godfrey, A. M. Loconsole, C. Holmes, and F. Prudenzano, "Effects of curvature on flexible Bragg grating in off-axis core: Theory and experiment," *J. Lightw. Technol.*, vol. 41, no. 9, pp. 2904–2910, May 2023.

[15] D. W. Mohammed, R. Waddingham, A. J. Flewitt, K. A. Sierros, J. Bowen, and S. N. Kukureka, "Mechanical properties of amorphous indium–gallium–zinc oxide thin films on compliant substrates for flexible optoelectronic devices," *Thin Solid Films*, vol. 594, pp. 197–204, Nov. 2015.

[16] H. Zhang, S. M. Eaton, and P. R. Herman, "Single-step writing of Bragg grating waveguides in fused silica with an externally modulated femtosecond fiber laser," *Opt. Lett.*, vol. 32, no. 17, pp. 2559–2561, 2007.

[17] G. Andria, F. Attivissimo, A. Di Nisio, A. M. L. Lanzolla, and M. A. Ragolia, "Assessment of position repeatability error in an electromagnetic tracking system for surgical navigation," *Sensors*, vol. 20, no. 4, p. 961, Feb. 2020.

[18] C. Holmes, M. Godfrey, P. L. Mennea, S. Zahertar, and J. M. Dulieu-Barton, "Flexible photonics in low stiffness doped silica for use in fibre reinforced polymer composite materials," *Opt. Mater.*, vol. 134, Dec. 2022, Art. no. 113133.

[19] X. Zhong, C. Guan, G. Mao, J. Fu, Y. Liu, J. Shi, and L. Yuan, "Bending characteristics of a long-period fiber grating in a hollow eccentric optical fiber," *Appl. Opt.*, vol. 54, no. 26, pp. 7879–7883, 2015.

[20] J. H. Osório, R. Oliveira, S. Aristilde, G. Chesini, M. A. R. Franco, R. N. Nogueira, and C. M. B. Cordeiro, "Bragg gratings in surface-core fibers: Refractive index and directional curvature sensing," *Opt. Fiber Technol.*, vol. 34, pp. 86–90, Mar. 2017.

[21] C. Holmes, M. Godfrey, D. J. Bull, and J. Dulieu-Barton, "Real-time through-thickness and in-plane strain measurement in carbon fibre reinforced polymer composites using planar optical Bragg gratings," *Opt. Lasers Eng.*, vol. 133, Oct. 2020, Art. no. 106111.
[22] C. Holmes, M. Godfrey, P. L. Mennea, D. J. Bull, and J. Dulieu-Barton, "Optical switching in glass fibre composite," *Opt. Laser Technol.*, vol. 152, Aug. 2022, Art. no. 108105.
[23] T. Erdogan, "Fiber grating spectra," *J. Lightw. Technol.*, vol. 15, no. 8, pp. 1277–1294, 1997.
[24] I. H. Malitson, "Interspecimen comparison of the refractive index of fused silica," *J. Opt. Soc. Amer.*, vol. 55, no. 10, pp. 1205–1208, 1965.
[25] A. Öchsner, "Euler–Bernoulli beam theory," in *Classical Beam Theories of Structural Mechanics*, 1st ed. Cham, Switzerland: Springer, 2021, pp. 7–66.
[26] A. Taghipour, A. Rostami, M. Bahrami, H. Baghban, and M. Dolatyari, "Comparative study between LPFG- and FBG-based bending sensors," *Opt. Commun.*, vol. 312, pp. 99–105, Feb. 2014.
[27] P. Kiiveri, M. Kuusisto, J. Koponen, O. Kimmelma, V. Aallos, J. Harra, H. Husu, and P. Kyllönen, "Refractive index profiles and propagation losses in bent optical fibers," *Opt. Eng.*, vol. 61, no. 12, Dec. 2022, Art. no. 126106.
[28] F. Anelli, A. Annunziato, A. Erario, C. Holmes, C. Ciminelli, and F. Prudenzano, "Design of microstructured flat optical fiber for multiaxial strain monitoring in composite materials," *J. Lightw. Technol.*, vol. 40, no. 17, pp. 5986–5994, Sep. 2022.
[29] C. Holmes, J. C. Gates, L. G. Carpenter, H. L. Rogers, R. M. Parker, P. A. Cooper, S. Chaotan, F. R. Mahamd Adikan, C. B. E. Gawith, and P. G. R. Smith, "Direct UV-written planar Bragg grating sensors," *Meas. Sci. Technol.*, vol. 26, no. 11, Nov. 2015, Art. no. 112001.
[30] A. Sun and Z. Wu, "Multimode interference in single mode-multimode FBG for simultaneous measurement of strain and bending," *IEEE Sensors J.*, vol. 15, no. 6, pp. 3390–3394, Jun. 2015.
[31] J. Ge, A. E. James, L. Xu, Y. Chen, K.-W. Kwok, and M. P. Fok, "Bidirectional soft silicone curvature sensor based on off-centered embedded fiber Bragg grating," *IEEE Photon. Technol. Lett.*, vol. 28, no. 20, pp. 2237–2240, Oct. 15, 2016.
[32] X. Chen, C. Zhang, D. J. Webb, K. Kalli, and G.-D. Peng, "Highly sensitive bend sensor based on Bragg grating in eccentric core polymer fiber," *IEEE Photon. Technol. Lett.*, vol. 22, no. 11, pp. 850–852, Jun. 2010.
[33] M. Hou, K. Yang, J. He, X. Xu, S. Ju, K. Guo, and Y. Wang, "Two-dimensional vector bending sensor based on seven-core fiber Bragg gratings," *Opt. Exp.*, vol. 26, no. 18, pp. 23770–23781, 2018.
[34] W. Zhou, Y. Zhou, X. Dong, L.-Y. Shao, J. Cheng, and J. Albert, "Fiber-optic curvature sensor based on cladding-mode Bragg grating excited by fiber multimode interferometer," *IEEE Photon. J.*, vol. 4, no. 3, pp. 1051–1057, Jun. 2012.

ANDREA ANNUNZIATO received the M.Sc. degree (cum laude) in electronic engineering from Politecnico di Bari, Bari, Italy, in 2020, where he is currently pursuing the Ph.D. degree in aerospace sciences and engineering. His research interests include the design and the characterization of silica optical fiber grating sensors based on planar substrate and flat fiber for curvature, strain, and temperature detection, also in reinforced polymer materials; and fluoride and chalcogenide fused optical fiber components, such as couplers and combiners for all-in-fiber amplifiers and lasers in the mid-infrared spectral range.

MIKE GODFREY received the bachelor's degree in mechanical engineering, in 2019, and the Ph.D. degree in biomedical engineering from the University of Southampton. His research has focused primarily on experimental mechanics and novel applications for full-field strain measurement. Although this is usually-based in the biomedical field, specifically next-generation orthopaedic implant design, his experience extends to composite materials and optical sensing. In the latter, his work has involved fibre Bragg gratings in single mode fibre, multimode Bragg gratings in custom optical chips and flat fibre, Rayleigh backscatter distributed fibre optic sensing (DFOS), and distributed acoustic sensing (DAS).

FRANCESCO ANELLI (Student Member, IEEE) received the M.Sc. degree (cum laude) in electronic engineering from Politecnico di Bari, Bari, Italy, in 2021, where he is currently pursuing the Ph.D. degree in electrical and information engineering. His research interests include the design and the characterization of silica optical fiber grating sensors based on novel geometries for curvature, strain, and temperature monitoring; and fluoride and chalcogenide fused optical fiber components, such as couplers and combiners for mid-infrared applications.

JANICE DULIEU-BARTON received the Ph.D. degree from Manchester University, in 1993, with a focus on thermoelastic stress analysis. She is currently a Full Professor of experimental mechanics with the Bristol Composites Institute, University of Bristol, where she is also the Director of the Industrial Doctorate Centre in Composites Manufacture. She has published around 450 articles with 140 in archival journals. Her expertise is in imaging for data rich material characterizations and structural integrity assessments, with a focus on lightweight structural design particularly composite structures. She has won numerous grants that have allowed her to develop novel approaches in experimental mechanics, most recently focusing on integration of flexible photonics into composite structures with colleagues with the University of Southampton.

CHRISTOPHER HOLMES is currently a Royal Society Industry Fellow with GE Aviation and a Principal Enterprise Fellow with the Optoelectronics Research Centre, University of Southampton, Southampton, U.K. He is also the Principal Investigator with the U.K. Engineering and Physical Science Research Council (EPSRC), developing new flexible silica planar optics, captured in this work. He is the Chair of Optica (formally Optical Society of America) Technical Group, on optical fabrication and testing, and an Associate Editor of *IET Science, Measurement and Technology*.

FRANCESCO PRUDENZANO (Member, IEEE) received the Ph.D. degree in electronic engineering from Politecnico di Bari, Bari, Italy, in November 1996. Since 2018, he has been a Full Professor of electromagnetic fields with the Department of Electrical and Information Engineering, Politecnico di Bari. He is currently the Head of Microwave and Optical Engineering Group, Department of Electrical and Information Engineering, Politecnico di Bari. He has coauthored more than 400 publications, 295 of which got published in journals and international conferences, lectures, and invited articles. He is involved in several national and international research projects and cooperations. His research interests include the design and characterization of microwave devices, integrated optics, and optical fiber-based devices. From 2017 to 2018, he was the Chair of SIOF, Italian Society of Optics and Photonics (Italian Branch of EOS—European Optical Society).

Open Access funding provided by 'Politecnico di Bari' within the CRUI CARE Agreement